

Trade-off Study for Proximity Approaches of Active Debris Removal Satellites: V-bar Hopping vs. Spiral Approach

デブリ接近軌道のトレードオフ評価: V-bar ホッピング軌道 vs スパイラル軌道 *

Takahiro SASAKI,¹⁾ Yu NAKAJIMA,¹⁾ and Toru YAMAMOTO¹⁾

佐々木 貴広,¹⁾ 中島 悠,¹⁾ 山元 透¹⁾

¹⁾Research and Development Directorate, JAXA, 宇宙航空研究開発機構 研究開発部門

The problems posed by orbital debris tend to become more serious with the increasing amount of space debris. It has become a global challenge for all nations associated with space. To solve such crucial problems, active debris removal missions are receiving much attention. In such missions, satellites should approach debris that are non-cooperative targets. However, such an approach is difficult when considering trajectory safety that ensures passive abort (PA) safety, even if some navigation sensors or control actuators should fail. This paper introduces two types of trajectories (V-bar hopping approach and spiral approach) in considering trajectory safety. For these two trajectories, the amount of ΔV budget, duration of operations, and required attitude rate relative to the navigation sensors through numerical simulations. The robustness to off-nominal thruster burn is also demonstrated through Monte Carlo simulation.

宇宙デブリの自然増加は深刻な問題となっており、各国の宇宙機関がデブリ増加の抑制に高い関心を示している。様々な積極的デブリ除去ミッションが提案されているが、非協力ターゲットへのランデブ接近技術は一つの大きな課題である。そこで本研究では、1km から 100m までのデブリ近傍における衛星の接近軌道について、V-bar 上をホップしながら接近する V-bar ホッピング軌道と V-bar を中心に螺旋状に接近するスパイラル軌道の 2 つの接近手法におけるトレードオフ評価を行う。数値シミュレーションを通して、燃料消費量、センサ要求、アクチュエータが故障時のロバスト性などの観点からトレードオフ評価を行い、比較および考察する。

1. Introduction

The problems posed by orbital debris tend to become more serious with the increasing amount of space debris. It has become a global challenge for all nations associated with space. To solve such crucial problems, active debris removal (ADR) missions are receiving much attention. In such missions, satellites should approach debris that are non-cooperative targets. However, such an approach is difficult when considering trajectory safety that ensures passive abort (PA) safety, even if some navigation sensors or control actuators should fail. This paper introduces two types of trajectories (V-bar hopping approach and spiral approach) in considering trajectory safety.

This paper first considers the V-bar hopping trajectory. There are several guidance methods for the R-bar or V-bar approach for ADR and rendezvous spacecraft. In terms of the amount of fuel consumption, this paper focuses on a V-bar approach. For such a V-bar approach, tangential boost maneuvers can move the satellite with lower fuel consumption, but control accuracy is not so high. The straight-line forced motion on the V-bar is both accurate and reliable, though it consumes much fuel to cancel the radial acceleration induced due to orbital dynamics. The V-bar hopping approach¹⁾ would be the most balanced for the removal satellite in terms of PA safety and fuel consumption.

This paper then considers the spiral trajectory. This approach considers relative orbit elements (ROEs) between the

ADR satellite and debris. It designs the trajectory with eccentricity/inclination (e/i)-vector separation²⁾ and also easily considers the PA safety of satellites geometrically.

For these two trajectories, this paper introduces orbital dynamics, control maneuvers, and abort characteristics of the V-bar hopping and spiral approaches, respectively, and then compares the amount of ΔV budget, duration of operations, and required attitude angles relative to the navigation sensors through numerical simulations. The robustness to off-nominal thruster burn is also demonstrated through Monte Carlo simulation.

2. Problem Statements

This paper focuses on the proximity approaches of ADR satellites from 1 km to 100 m, while minimizing the risk of collision and off-nominal thruster burn. Since a delay in detecting mechanical failure is critical in a proximity operation, PA safety would be an important factor in this rendezvous phase when a satellite approaches a non-cooperative target such as a space debris.

LVLH, RTN, and RVH-bar coordinates are defined as each axis at the origin of the target's center of mass as shown in Fig. 1. In defining the safe region that satellites can approach, the Keep-Out-Sphere (KOS) should be set as a red sphere in Fig. 1. KOS is defined as an area where a satellite is not allowed to enter when approaching a target. However, the proximity approaches of satellites entail GNC error (i.e., noise

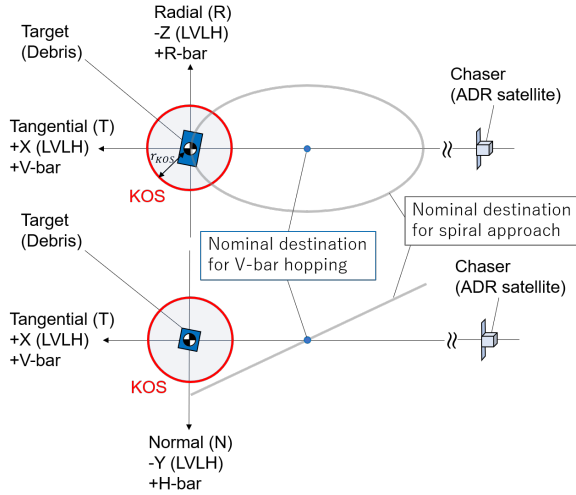


Fig. 1. Definition of coordinates, KOS, and nominal destination

in the navigation sensors), thruster maneuver error (i.e., excessive or insufficient thruster burn), control input delay, and estimation error regarding orbit and attitude determinations. Therefore, nominal destinations for a V-bar hopping and a spiral approach should be set while considering a margin as shown in Fig. 1.

3. Trajectory Design

This paper introduces two types of trajectories (V-bar hopping approach and spiral approach) in considering trajectory safety.

3.1. V-bar Hopping Approach

The V-bar hopping approach would be the most balanced for the removal satellite in terms of PA safety and fuel consumption, where the satellite moves a predefined distance with stepwise small ΔV impulses at the V-bar in the radial direction.

HCW equation:

If the orbit of the target debris is a circle, a Hill-Clohesy-Wiltshire (HCW) equation is a useful representation for calculating the required ΔV . Since a V-bar hopping approach does not include out-of-plane ($\pm y$) motion, a HCW equation can be simplified to

$$\begin{bmatrix} \mathbf{x}_{xz}(\Delta t) \\ \mathbf{v}_{xz}(\Delta t) \end{bmatrix} = \begin{bmatrix} \Theta_{11}(\Delta t) & \Theta_{12}(\Delta t) \\ \Theta_{21}(\Delta t) & \Theta_{22}(\Delta t) \end{bmatrix} \begin{bmatrix} \mathbf{x}_{xz}(0) \\ \mathbf{v}_{xz}(0) \end{bmatrix} \quad (1)$$

where

$$\Theta_{11}(\Delta t) = \begin{bmatrix} 1 & 6(\omega\Delta t - \sin \omega\Delta t) \\ 0 & 4 - 3 \cos \omega\Delta t \end{bmatrix}, \quad (2)$$

$$\Theta_{12}(\Delta t) = \begin{bmatrix} \frac{1}{\omega}(4 \sin \omega\Delta t - 3\omega\Delta t) & \frac{2}{\omega}(1 - \cos \omega\Delta t) \\ -\frac{2}{\omega}(1 - \cos \omega\Delta t) & \frac{\sin \omega\Delta t}{\omega} \end{bmatrix}, \quad (3)$$

$$\Theta_{21}(\Delta t) = \begin{bmatrix} 0 & 6\omega(1 - \cos \omega\Delta t) \\ 0 & 3\omega \sin \omega\Delta t \end{bmatrix}, \quad (4)$$

$$\Theta_{22}(\Delta t) = \begin{bmatrix} 4 \cos \omega\Delta t - 3 & 2 \sin \omega\Delta t \\ -2 \sin \omega\Delta t & \cos \omega\Delta t \end{bmatrix} \quad (5)$$

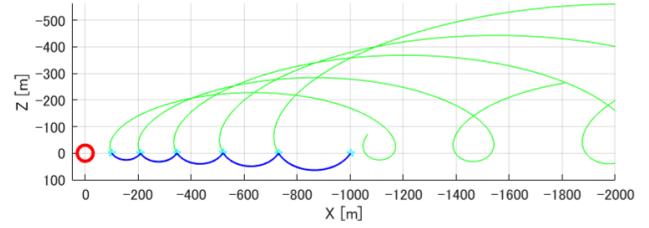


Fig. 2. Failed maneuver analysis of a V-bar hopping.

together with $\mathbf{x}_{xz} = [x, z]^T$, $\mathbf{v}_{xz} = [v_x, v_z]^T$, and ω is orbital rate of the target. Using Eq. (1), the required $\Delta V (= \mathbf{v}_{xz}(0))$ which achieves the desired position $\mathbf{x}_{xz}(\Delta t)$ in Δt s is obtained by

$$\mathbf{v}_{xz}(0) = \Theta_{12}^{-1}(\Delta t) (\mathbf{x}_{xz}(\Delta t) - \Theta_{11}(\Delta t)\mathbf{x}_{xz}(0)). \quad (6)$$

Note that V-bar hopping usually assumes $z(0) = z(\Delta t) = 0$ (at the point on the V-bar). This equation provides a numerical solution set of the required ΔV . If $\text{rank}(\Theta_{12}(\Delta t)) = 2$, the inverse matrix $\Theta_{12}^{-1}(\Delta t)$ can be always obtained. However, if the $\text{rank}(\Theta_{12}(\Delta t)) \neq 2$ then this cannot be solved. It occurs when $\det(\Theta_{12}(\Delta t)) = 0$ or equivalently

$$8(1 - \cos \omega t) - 3\omega t \sin \omega t = 0. \quad (7)$$

Parameter design policy:

Based on the reference,¹⁾ assumptions for designing the parameters are given as follows:

- Total hopping time t_{total} can be designed according to the mission.
- One hopping time is equivalently set to Δt considering the number of hopping n_{hop} .
- The hopping interval is shortened at the constant rate γ_{hop} (hopping rate).

Note that the number of hopping n_{hop} is determined by

$$n_{hop} = \begin{cases} n_{hop,min} & \left(\frac{t_{total}}{\Delta t} < n_{hop,min} \right) \\ \left\lfloor \frac{t_{total}}{\Delta t} \right\rfloor & \left(\frac{t_{total}}{\Delta t} \geq n_{hop,min} \right) \end{cases}. \quad (8)$$

Note that $\lfloor \mathcal{A} \rfloor$ represents the floor function that takes as input a real number \mathcal{A} and gives as output the greatest integer less than or equal to \mathcal{A} . When one or two hopping approach is adopted, there is a high probability that a satellite will enter the KOS. Therefore, the minimum hopping number $n_{hop,min}$ is defined by the GNC error, thruster maneuver error, and so on.

Example:

Figure 2 shows an example of free-drift trajectories after maneuver failure in a nominal trajectory of the V-bar hopping approach. The blue line shows the nominal trajectory of a V-bar hopping and the green lines show the off-nominal trajectories after maneuver failures. In this figure, PA is successfully achieved when total hopping time $t_{total} = 1$ rev (= 6000 s).

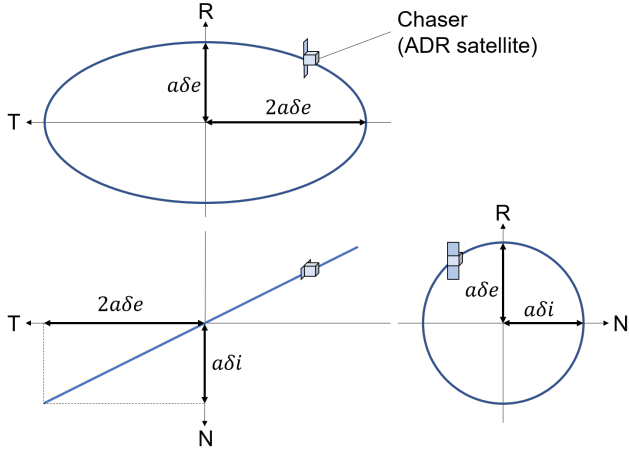


Fig. 3. Configuration of a spiral motion

3.2. Spiral Approach

The spiral approach (sometimes called “e/i-vector separation”) is described as relative orbit elements (ROEs) constructed by the eccentricity and inclination vectors. The trajectory runs spirally along the V-bar. The concept of the spiral approach is derived from the aforementioned linearized relative motion model and can be used to design proximity operation geometries characterized by passive safety and stability.²⁾

Relative orbit elements:

ROEs $\delta\alpha$ are an useful representation to describe the relative orbit, and are defined as follows:

$$\delta\alpha = \begin{bmatrix} \delta a \\ \delta\lambda \\ \delta e_x \\ \delta e_y \\ \delta i_x \\ \delta i_y \end{bmatrix} = \begin{bmatrix} \Delta a/a \\ \Delta u + \Delta\Omega \cos i \\ \Delta e_x \\ \Delta e_y \\ \Delta i \\ \Delta\Omega \sin i \end{bmatrix} \quad (9)$$

with relative eccentricity vector δe and relative inclination vector δi being defined as follows:

$$\delta e = \begin{bmatrix} \delta e_x \\ \delta e_y \end{bmatrix} = \delta e \begin{bmatrix} \cos \phi \\ \sin \phi \end{bmatrix}, \quad \delta i = \begin{bmatrix} \delta i_x \\ \delta i_y \end{bmatrix} = \delta i \begin{bmatrix} \cos \theta \\ \sin \theta \end{bmatrix} \quad (10)$$

where a is the semi-major axis, and e and i are eccentricity and inclination, respectively. Parameters Ω , u , and λ are right ascension of ascending node, mean argument of latitude, and mean longitude, respectively. Note that the phases of the relative e/i vectors in Eq. (10) are termed relative perigee ϕ and relative ascending node θ . ROEs can be geometrically characterized as shown in Fig. 3.

Gauss equation:

The Gauss equation provides the consequent change of ROEs from an impulsive maneuver as follows:

$$\Delta(a\delta\alpha) = \Delta \begin{bmatrix} a\delta a \\ a\delta\lambda \\ a\delta e_x \\ a\delta e_y \\ a\delta i_x \\ a\delta i_y \end{bmatrix} = \frac{1}{\omega} \begin{bmatrix} 0 & 2 & 0 \\ -2 & 0 & 0 \\ \sin u & 2 \cos u & 0 \\ -\cos u & 2 \sin u & 0 \\ 0 & 0 & \cos u \\ 0 & 0 & \sin u \end{bmatrix} \begin{bmatrix} \Delta v_R \\ \Delta v_T \\ \Delta v_N \end{bmatrix}. \quad (11)$$

From this equation, the in-plane and out-of-plane relative motions are decoupled. Maneuvers in radial or tangential direction affect the eccentricity vector. Although tangential maneuvers are twice as efficient as radial maneuvers in terms of propellant consumption, these maneuvers also affect the semi-major axis. Maneuvers in a normal direction only affect the inclination vector, which controls the out-of-plane motion. For bounded relative motion ($\delta a = 0$), the minimum collision risk is provided by parallel or anti-parallel relative e/i-vectors.

Relative orbit control maneuvers:

Orbital control maneuvers in the normal direction for out-of-plane reconfiguration are given by

$$\Delta v_N = v \|\Delta i\| \quad (12)$$

where

$$u = \arctan(\Delta\delta i_y / \Delta\delta i_x). \quad (13)$$

Orbital control maneuvers in the tangential direction for in-plane reconfiguration with spiral motion are given by

$$\Delta v_T^1 = +\frac{v}{4} (\|\Delta e\| + \|\Delta a/a\|) \quad (14)$$

$$\Delta v_T^2 = -\frac{v}{4} (\|\Delta e\| - \|\Delta a/a\|) \quad (15)$$

where

$$u^1 = \arctan(\Delta\delta e_y / \Delta\delta e_x) \quad (16)$$

$$u^2 = u^1 + \pi \quad (17)$$

for the maneuver locations, respectively. Orbital control maneuvers in the radial direction for in-plane reconfiguration without spiral motion are given by

$$\Delta v_R^1 = +\frac{v}{4} (2\|\Delta e\| + \|\Delta\delta\lambda\|) \quad (18)$$

$$\Delta v_R^2 = -\frac{v}{4} (2\|\Delta e\| - \|\Delta\delta\lambda\|) \quad (19)$$

where

$$u^1 = \arctan(\Delta\delta e_y / \Delta\delta e_x) + \pi/2 \quad (20)$$

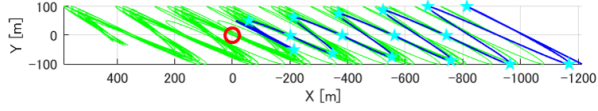
$$u^2 = u^1 + \pi \quad (21)$$

for the maneuver locations, respectively.

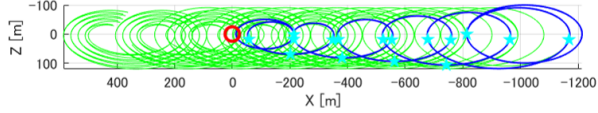
Parameter design policy:

To design the parameters, the following assumptions apply:

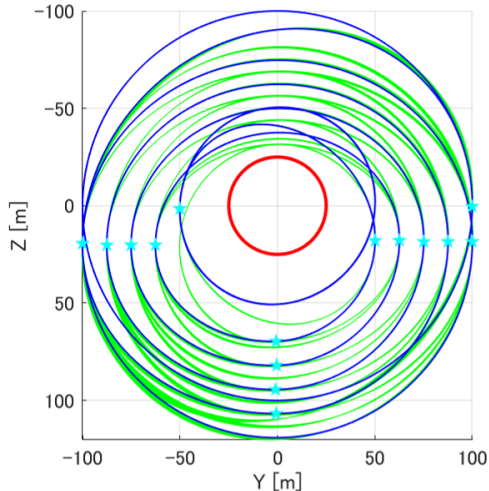
- The trajectory in the R-N plane is described as a circle ($\delta e = \delta i$).
- δe and δi in the initial relative orbit is twice larger than those of the nominal destination.
- The spiral motion become smaller by the constant value Δe and Δi .
- The number of spiral motion n_{spiral} depends on the duration of operation.



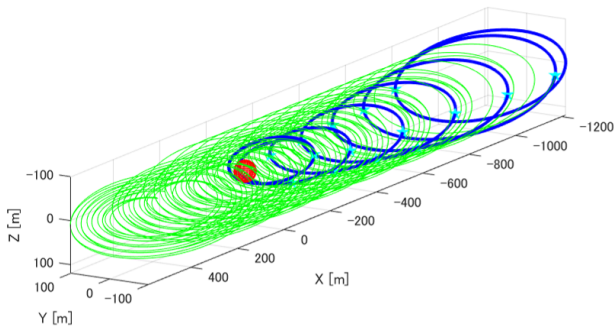
(a) Spiral approach (X-Y).



(b) Spiral approach (X-Z).



(c) Spiral approach (Y-Z).



(d) Spiral approach (3D).

Fig. 4. Failed maneuver analysis of a spiral approach.

Example:

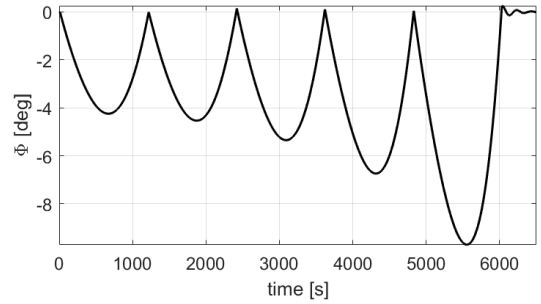
Through failed maneuver analysis, PA safety of the spiral approach is demonstrated in Fig. 4. The blue line shows the nominal trajectory of a spiral approach and the green lines show the off-nominal trajectories after maneuver failures. In this figure, spiral motion passes by the target debris with a spiral trajectory around the origin as a point on the V-bar.

4. Numerical Simulations

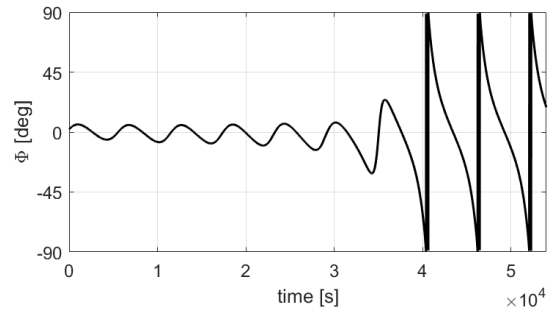
This section compares the amount of ΔV budget, duration of operations, and required FOV to the navigation sensors of two trajectories through numerical simulations. Then robustness to off-nominal thruster burn is also demonstrated

Table 1. Comparison of ΔV budget in two trajectories.

| t_{total} [rev] | V-bar hopping | | Spiral | |
|-------------------|---------------|------------------|--------------|------------------|
| | n_{hop} | ΔV [m/s] | n_{spiral} | ΔV [m/s] |
| 1.0 | 5 | 1.6112 | - | - |
| 1.5 | 6 | 1.2881 | 1 | 0.21093 |
| 2.0 | 8 | 1.2756 | - | - |
| 2.5 | 10 | 1.2662 | 2 | 0.15941 |
| 3.0 | 12 | 1.2584 | - | - |
| 3.5 | 14 | 1.2558 | 3 | 0.14224 |
| 4.0 | 16 | 1.2542 | - | - |
| 4.5 | 18 | 1.2532 | 4 | 0.13365 |
| 5.0 | 20 | 1.2519 | - | - |
| 5.5 | 22 | 1.2524 | 5 | 0.12850 |



(a) Target direction with V-bar hopping.



(b) Target direction with spiral approach.

Fig. 5. Comparison of the target directions.

through Monte Carlo simulation.

4.1. Comparison of ΔV budget

This subsection compares the amount of ΔV budget in a V-bar hopping and a spiral approach. Table 1 shows the total ΔV budget for each duration of operation. In this table, the amount of ΔV budget of the spiral approach is much less than that of the V-bar hopping approach. On the other hand, unlike a spiral approach, a V-bar hopping approach has the advantage of a flexible duration of operation by choosing the number of hopping properly. The number of hopping is determined by Eq (8).

4.2. Comparison of navigation requirements

This subsection compares directions of target debris as a navigation requirement. FOV constraints of navigation sensors (e.g., optical camera or 3D LiDAR) are also compared. Figure 5 shows the relative positions which are the direction

of the target debris from the ADR satellites, as obtained by

$$\Phi = \arctan\left(\frac{z_{rel}^{LVLH}}{x_{rel}^{LVLH}}\right). \quad (22)$$

The maximum direction angle of the V-bar hopping approach is much less than that of the spiral one. Figure 5 (a) presents the target direction angle is less than 10 deg, which implies attitude control with optical camera whose FOV is greater than 10 deg is easy to be achieved without relative navigation.

4.3. Monte Carlo Simulation

Figures 6 and 8 show the Monte Carlo simulation results of two PA safe trajectories. To clarify the property of the robustness to the excessive and insufficient maneuvers, a thruster burn with uncertainty as standard uniform distribution $\gamma \sim U(0, 2)$ is given by

$$\Delta V_{thr} \sim \gamma \cdot \Delta V_{true} \quad (23)$$

where

$$\gamma = \begin{cases} 0 & : \text{passive abort} \\ \hat{\gamma}, \quad 0 < \hat{\gamma} < 1 & : \text{insufficient maneuver} \\ 1 & : \text{required maneuver} \\ \tilde{\gamma}, \quad \tilde{\gamma} > 1 & : \text{excessive maneuver} \end{cases} \quad (24)$$

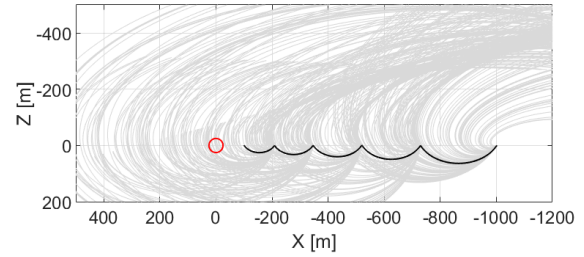
at each maneuvers point. Note that γ describes the off-nominal rate. Once off-nominal maneuver is executed, thruster burn is not executed anymore to check the safety of the trajectories. From Fig. 6, the V-bar hopping approach entered the KOS area. Figure 7 shows that the relationship between off-nominal rate and the maneuver number with off-nominal thruster burn. From this figure, excessive maneuvers in a V-bar hopping approach may lead to the invasion especially in the case of the maneuver near debris. On the other hand, there is no case that satellites in spiral approaches invade the KOS. Therefore, the spiral approach has robustness to off-nominal thruster burn as compared with the V-bar hopping approach.

4.4. Discussions

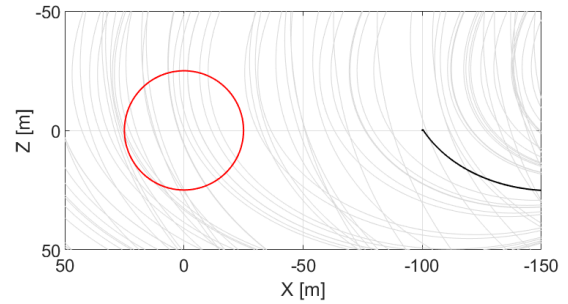
As for a V-bar hopping approach, it has the advantage of easily observing the target, thanks to a simple attitude tracking rate that only depends on the pitch angle from LVLH coordinates and FOV constraints of navigation sensors (e.g. optical cameras or LiDARs) is not strict. On the other hand, as for a spiral approach, it has the advantages of only requiring small ΔV , robustness to off-nominal thruster burn as compared with the V-bar hopping approach, and FOV constraints of navigation sensors is strict. Trajectory safety which is partially guaranteed by robustness to the thruster error has an impact on non-cooperative rendezvous such as ADR missions. However, FOV constraints leads to strict constraints of satellite's systems such as GNC sensors, power, thermal, and communication. Furthermore, it will be difficult to achieve Line-of-sight (LoS) control to the target debris.

5. Conclusion

This paper introduces and develops the orbital dynamics, control maneuvers, and abort characteristics of two passive abort safe trajectories the V-bar hopping approach and the



(a) V-bar hopping (X-Z plane).



(b) V-bar hopping (X-Z plane, magnified).

Fig. 6. Monte Carlo simulations at each maneuver point with V-bar hopping

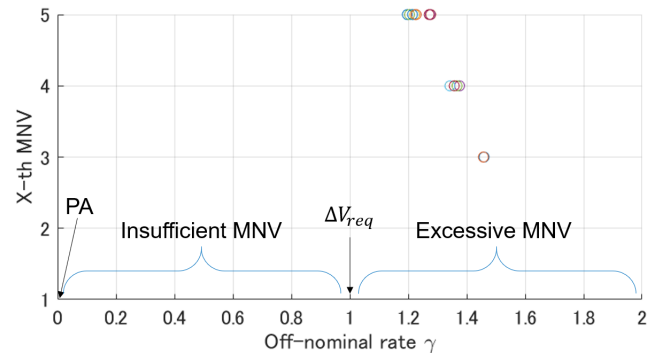


Fig. 7. Invasions of KOS.

spiral approach. It then compares the amount of ΔV budget, duration of operations, and required relative attitude angles to the navigation sensors through numerical simulations. The robustness to off-nominal thruster burn is also demonstrated through Monte Carlo simulation. As a result, it is shown that the V-bar hopping approach has the advantage of easily observing the target, thanks to small required relative attitude, whereas the spiral approach has the advantages of a small ΔV to achieve a proximity approach and robustness to off-nominal thruster burn.

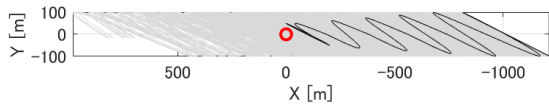
Acknowledgment

This work was supported by JSPS Grant-in-Aid for Scientific Research Grant Number 19K15020.

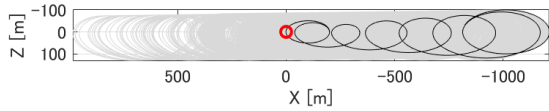
References

- 1) Murakami, N. and Yamamoto, T.: Navigation System and Trajectory Analysis for Active Debris Removal Mission, AAS/AIAA Astrodynamics Specialist Conference, AAS 17-574, 2017.

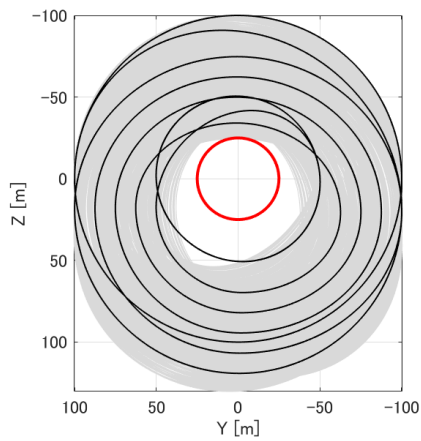
- 2) D'Amico, S. and Montenbruck, O.: Proximity Operations of Formation-Flying Spacecraft Using an Eccentricity/Inclination Vector Separation, *J. Guid., Control Dynam.*, **29** (2006), pp. 554–563.



(a) Spiral approach (X-Y plane).



(b) Spiral approach (X-Z plane).



(c) Spiral approach (Y-Z plane).

Fig. 8. Monte Carlo simulations at each maneuver point with spiral approach.